

MAGNETIC STAR-DISK COUPLING IN CLASSICAL T TAURI SYSTEMS

MANFRED KÜKER,^{1,2} THOMAS HENNING,^{1,3} AND GÜNTHER RÜDIGER²

Received 2002 August 21; accepted 2003 January 28

ABSTRACT

We study the interaction between a dipolar magnetic field rooted in the central star and the circumstellar accretion disk in a classical T Tauri system. The MHD equations, including radiative energy transport, are solved for an axisymmetric system with a resistive, turbulent gas. A Shakura-Sunyaev-type eddy viscosity and a corresponding eddy magnetic diffusivity are assumed for the disk. The computations cover the disk and its halo in a radial interval from 1.7 to 20 stellar radii. The initial magnetic field configuration is unstable. Because of magnetocentrifugal forces caused by the rotational shear between star and disk, the magnetic field is stretched outward and part of the field lines open. For a solar-mass pre-main-sequence star and an accretion rate of $10^{-7} M_{\odot} \text{ yr}^{-1}$, a dipolar field of 1 kG (on the stellar surface) is not sufficient to disrupt the disk. The outer, slowly rotating parts of the disk become disconnected, and about 1/10 of the accretion flow is lost because of an outflow at midlatitudes. The critical field strength for the disruption of the disk lies between 1 and 10 kG. Outflows occur at midlatitudes, with mass fluxes of the order of 10% of the accretion rate of the disk. We find solutions in which the magnetic field tends to spin down the stellar rotation without disk disruption, but in these cases the accretion torque is dominant, and the star is still spun-up.

Subject headings: accretion, accretion disks — circumstellar matter — MHD — stars: magnetic fields — stars: pre-main-sequence — stars: variables: other

On-line material: color figures

1. INTRODUCTION

A number of T Tauri stars show evidence for the presence of magnetic fields with surface strengths of several kilogauss (Guenther & Emerson 1996; Guenther et al. 1999; Johns-Krull, Valenti, & Koresko 1999). In a classical T Tauri system (CTTS), in which a pre-main-sequence star is surrounded by an accretion disk, the inner parts of that disk are then threaded by the stellar magnetic field. A sufficiently strong magnetic field should not only change the structure of the inner parts of the disk but also transfer a significant amount of angular momentum between the star and the disk. Magnetic coupling between the central T Tauri star and a truncated disk has been proposed to be the mechanism that prevents T Tauri stars from spinning up to breakup velocity during the contraction toward the main sequence (Cameron & Campbell 1993; Yi 1994; Armitage & Clarke 1996; Li, Wickramasinghe, & Rüdiger 1996; Bouvier, Forestini, & Allain 1997). The rotation periods typically lie between 0.1 and 8 days. The disk-locking scenario predicts weak-line TTSSs to rotate faster than CTTSs, because of the lack of a disk. While some observations seem to support that picture (Bouvier et al. 1993; Edwards et al. 1993; Ghosh 1995), others favor a single-moded distribution and thus show no evidence for a coupling between stars and their disks in CTTSs (Stassun et al. 1999, 2001).

The coupling between an accretion disk and its central object was first discussed by Ghosh & Lamb (1978, 1979a, 1979b). In their model of an accreting neutron star, the dipolar magnetic field of the rotating star threads the sur-

rounding disk. As the toroidal field generated by the rotational shear between the star and disk reverses its sign at the corotation radius, so does the torque exerted on the disk. Inside the corotation radius, the magnetic field transfers angular momentum from the disk to the star, while the outer parts of the disk, which rotate slower than the star, brake the stellar rotation. Because of the rapid decrease of the field strength with radius, the inner parts dominate and the star is spun-up unless the inner edge of the disk lies very close to the corotation radius. Between the stellar surface and the corotation radius the accretion flow follows the magnetic field, and no disk exists. In this way a further spin-up of the star is avoided, and a decelerating torque can be exerted on the stellar surface.

The truncation radius is a crucial parameter of the disk-locking model. Ghosh & Lamb (1979a) find

$$R_t = \Gamma_t R_*, \quad \Gamma_t = \alpha_t \left(\frac{B_*^4 R_*^5}{GM_* \dot{M}^2} \right)^{1/7}, \quad (1)$$

where $\alpha_t < 1$ is a dimensionless parameter, B_* the field strength on the stellar surface, R_* the stellar radius, and \dot{M} the accretion rate. Elstner & Rüdiger (2000) studied a two-dimensional model in which the disk structure was treated in a one+one-dimensional approach, while the magnetic field was evolved using a two-dimensional induction solver assuming Keplerian rotation in and rigid corotation with the star above the disk. They found that for a field strength of 200 G or more, the disk is depleted because of enhanced accretion inside the corotation radius and eventually truncated at the latter.

The assumption of a purely dipolar field and a rigidly rotating halo above the disk appears unrealistic. The rotational shear between the two footpoints of a field line will cause an initially dipolar field threading a resistive disk to be stretched in the radial direction first, and then the footpoints to be pushed outward, away from the central star (Aly 1984;

¹ Astrophysikalisches Institut und Universitäts-Sternwarte, Schillergässchen 2-3, 07745 Jena, Germany.

² Astrophysikalisches Institut Potsdam, An der Sternwarte 16, 14482 Potsdam, Germany.

³ Max-Planck-Institut für Astronomie, Königstuhl 17, 69117 Heidelberg, Germany.

Lovelace, Romanova, & Bisnovaty-Kogan 1995; Bardou & Heyvaerts 1996; Agapitou & Papaloizou 2000).

Camenzind (1990), Königl (1991), Cameron & Campbell (1993), Shu et al. (1994), and Ghosh (1995) have applied the Ghosh & Lamb scenario to the problem of coupling a T Tauri star to the surrounding disk by a dipolar magnetic field. While the models of Königl (1991), Cameron & Campbell (1993), and Ghosh (1995) assume the dipole to be only weakly distorted, Camenzind (1990) and Shu et al. (1994) assume a force-free field above the disk with an accretion flow along the field lines close to the inner edge of the disk. They conclude that only the inner part of the disk is magnetically connected to the star, while the outer parts of the disk are threaded by open field lines.

For a reliable estimate of the total torque exerted on the central star, knowledge of both the structure of the magnetized disk and the field configuration in the medium above the disk is necessary. Uchida & Shibata (1985), Goodson, Winglee, & Böhm (1997), and Miller & Stone (1997) carried out two-dimensional simulations of magnetized disks, but the works of Uchida & Shibata and of Goodson, Winglee, & Böhm focused on the launching of jets, while Miller & Stone studied the formation of a funnel flow toward the poles of the central star. We therefore present a series of computations that involve a fully two-dimensional model of the disk structure as well as the evolution of an initially dipolar magnetic field rooted in the central star and threading the disk.

2. THE MODEL

With outer radii of several hundred AU, the ratio of the outer and inner radii of a protoplanetary disk is about 10^4 . For a dipolar magnetic field, the field strength decreases with the third power of the distance from the star. Therefore, only the innermost part of the disk is directly affected by the stellar magnetic field. As we focus on the star-disk interaction, we restrict our computations to that part of the disk and the halo above. The gas is assumed to be ionized and the degree of ionization to be sufficient for a single-fluid approach to hold. The system can then be described by a set of eight partial differential equations, namely, the conservation laws of mass,

$$\frac{\partial \rho}{\partial t} + \nabla \cdot (\rho \mathbf{u}) = 0, \quad (2)$$

momentum,

$$\rho \left[\frac{\partial \mathbf{u}}{\partial t} + (\mathbf{u} \cdot \nabla) \mathbf{u} \right] = -\nabla p + \mathbf{f} + \nabla \cdot \mathbf{T}, \quad (3)$$

and gas energy,

$$c_v \rho \left[\frac{\partial T}{\partial t} + (\mathbf{u} \cdot \nabla) T \right] = -p \nabla \cdot \mathbf{u} + \Phi_{\text{visc}} + \Phi_{\text{mag}} - \Lambda, \quad (4)$$

and the induction equation,

$$\frac{\partial \mathbf{B}}{\partial t} = \nabla \times (\mathbf{u} \times \mathbf{B} - \eta_t \nabla \times \mathbf{B} + \mathbf{u} \times \mathbf{B}_0). \quad (5)$$

In equation (3) the force term reads

$$\mathbf{f} = \rho \nabla \frac{GM_*}{r} + \rho \frac{\kappa + \sigma}{c} \mathbf{F}_0 + \frac{1}{4\pi} \nabla \times \mathbf{B} \times \mathbf{B}, \quad (6)$$

where \mathbf{T} denotes the stress tensor. In equation (4)

$$\Phi_{\text{visc}} = (\mathbf{T} \cdot \nabla) \cdot \mathbf{u} \quad (7)$$

denotes the viscous heating and

$$\Phi_{\text{mag}} = 4\pi \eta_t j^2, \quad (8)$$

with the electric current \mathbf{j} , is the magnetic heating term. In equation (6) the term containing the radiative energy flux \mathbf{F}_0 is the radiative force. It is only present in those cases in which radiation is included (see below). The same holds for the radiative cooling term in equation (4),

$$\Lambda = \rho c \kappa (aT^4 - E_0). \quad (9)$$

For a description of the stress tensor \mathbf{T} , see Klahr, Henning, & Kley (1999).

Throughout this work we assume axisymmetry. A time-dependent 2.5-dimensional finite-difference code for solving the equations of radiation hydrodynamics based on the method of constrained transport (Evans & Hawley 1988) has been developed by Kley (1989). Stone & Norman (1992a, 1992b) and Hawley & Stone (1995) describe a modification of the original Evans & Hawley scheme that ensures stability by interpolating the field advection and Lorentz force terms along the characteristics (method of characteristics with constrained transport). To treat the full MHD system of equations, the induction equation and Lorentz force terms as described in Stone & Norman (1992b) have been added to the Kley (1989) code, and an additional heating term due to the ohmic dissipation was included in the equation for the gas energy. As tests, the wind solution by Weber & Davis (1967) and the results of Stone & Norman (1994) were reproduced.

In the nonmagnetic case the disk is in hydrostatic equilibrium, and its vertical structure is determined by a local equilibrium between viscous heating and radiative cooling. For finding an appropriate initial mass distribution and very long runs, in which the thermal evolution of the disk is an issue, we include the equation for the radiation energy density, which is treated using the flux-limited diffusion approximation (Levermore & Pomraning 1981):

$$\frac{\partial E_0}{\partial t} + \nabla \cdot (E_0 \mathbf{u}) = \nabla \cdot \mathbf{F}_0 + \Lambda - \rho \frac{\kappa + \sigma}{c} \mathbf{u} \cdot \mathbf{F}_0, \quad (10)$$

where

$$\mathbf{F}_0 = -\frac{c\lambda}{\rho(\kappa + \sigma)} \nabla E_0, \quad (11)$$

$$\lambda = \frac{2 + \chi}{6 + 3\chi + \chi^2}, \quad (12)$$

$$\chi = \frac{1}{\rho(\kappa + \sigma)} \frac{|\nabla E_0|}{E_0}. \quad (13)$$

The *Ansatz* in equation (11) transforms the radiation energy equation (10) into a diffusion equation that is valid in the optically thin as well as in the optically thick case. For the opacity, an analytical approximation of the opacity tables by Alexander, Auguson, & Johnson (1989), derived by Bell & Lin (1994), is used.

We assume a perfect gas described by the equation of state

$$p = (n_e + \sum_i n_i) kT, \quad (14)$$

where n_e and n_i are the number densities of the electrons and ions, respectively. The number densities of the different types of ion are related through the Saha equation:

$$\frac{n_{i+1}}{n_i} = \frac{g_{i+1}}{g_i} f_s(T). \quad (15)$$

The code includes the ionization of hydrogen and helium. Note that the degree of ionization enters the model in the equation of state only. We always assume the molecular electric conductivity of the gas to be large enough for the MHD approach to hold.

The small-scale motions of the gas inside the disk are assumed to be subsonic and turbulent. Their effect on the large-scale flow is modeled by a turbulence viscosity,

$$\nu_T = \alpha_{SS} c_s H_p, \quad (16)$$

where $\alpha_{SS} < 1$ is a free parameter, c_s is the local sound speed, and H_p is the pressure scale height (Shakura & Sunyaev 1973). If the pressure scale height exceeds the height of the disk, the latter is used instead. With $\dot{M} = 10^{-7} M_\odot \text{ yr}^{-1}$ and $\alpha_{SS} = 0.01$, values between 10^{14} and $10^{15} \text{ cm}^2 \text{ s}^{-1}$ result for ν_T in the disk.

In turbulent conductive fluids the decay of large-scale electric and magnetic fields is strongly enhanced by small-scale motions. Provided the molecular electric conductivity is high and the small-scale velocity field is statistically isotropic, this enhanced decay can be described by a turbulent magnetic diffusivity η_T . Unlike the turbulence viscosity, which plays an essential part in the process of accretion, η_T cannot be directly derived from the global properties of the disk. Kitchatinov, Pipin, & Rüdiger (1994) computed both parameters using the second-order correlation approximation and found nearly identical values for slow rotation and isotropic, homogeneous turbulence:

$$\nu_T = \frac{4}{5} \tau_{\text{corr}} \langle u'^2 \rangle, \quad \eta_T = \frac{1}{3} \tau_{\text{corr}} \langle u'^2 \rangle, \quad (17)$$

where τ_{corr} is the correlation time and u' the amplitude of the velocity fluctuations. Lacking a detailed model for turbulence in accretion disks, we relate the turbulent magnetic diffusivity to the turbulence viscosity through the (turbulent) magnetic Prandtl number Pr_m :

$$\eta_T = \frac{\nu_T}{\text{Pr}_m}. \quad (18)$$

Equation (17) suggests $\text{Pr}_m = 1$, which we assume throughout this paper.

The molecular values for both the viscosity and the magnetic diffusivity can be neglected compared to the turbulent values, as long as the degree of ionization is high enough to justify the use of the MHD equations. Small but finite values are used for the viscosity (2 orders of magnitude smaller than in the disk) wherever the density drops below $10^{-12} \text{ g cm}^{-3}$, while the magnetic diffusivity is set to 0 in these areas.

The computations cover the disk itself and the halo above. The inner radius is located at 1.7 stellar radii, about one-third of the corotation radius, while a radius of 20 stellar radii is chosen for the outer boundary, such that the boundary conditions do not affect the inner parts, where the interaction between the stellar magnetic field and the disk occurs.

To generate the start solution, we switch the stellar magnetic field off and the radiation transport on. The

one-dimensional version of the original Kley code is then used with the same set of input parameters to solve for the vertical structure of the disk at the inner and outer radii of the two-dimensional integration volume. The initial disk is then generated by linear interpolation between these two one-dimensional solutions. The rotation rate is assumed Keplerian, the radial velocity is determined by the initial mass accretion rate, and the vertical velocity component is assumed to be 0.

While measurements of magnetic activity give an estimate for the field strength in the stellar photosphere, the field geometry is unknown. Since we assume axisymmetry throughout this paper, the most natural choice for the unperturbed stellar magnetic field is that of an axisymmetric dipole:

$$B_r = \frac{B_* \cos \theta}{r^3}, \quad B_\theta = \frac{B_* \sin \theta}{r^3}, \quad (19)$$

where r is to be taken in units of the stellar radius. The stellar magnetic field can be treated as either an initial or an external field.

The initial state consists of a disk interpolated from one-dimensional vertical structure models and a halo of thin perfectly conducting gas. The vertical structure models are computed with a one-dimensional radiation hydrodynamics code and show very steep density gradients in the atmosphere of the disk. A large density contrast between disk and halo is necessary to ensure that the disk is not significantly affected by purely mechanical interactions with the halo and infall of gas from the latter. The density distribution in the halo,

$$\rho = \rho_0 \left(\frac{R_0}{r} \right)^n, \quad (20)$$

where R_0 is the normalization radius (see below), contains the input parameters ρ_0 and n . With $\rho_0 = 10^{-12} \text{ g cm}^{-3}$ and $n = 2$, the density in the halo is about 4 orders of magnitude smaller than in the disk, where it varies between 10^{-8} and $10^{-10} \text{ g cm}^{-3}$. The initial temperature of the gas in the halo is 5000 K, while the maximum temperature in the disk is 7000 K. The gas in the halo is initially at rest, while the disk rotates Keplerian everywhere. The stellar magnetic field penetrates the disk; i.e., we start with a purely dipolar field.

In all runs the stellar rotation rate was 1/10 of the breakup rotation rate

$$\Omega_K = \sqrt{\frac{GM_*}{R_*^3}}. \quad (21)$$

With $G = 6.67 \times 10^{-8} \text{ g}^{-1} \text{ cm}^3 \text{ s}^{-2}$, the breakup rotation frequency is $\Omega_K = 1.3 \times 10^{-4} \text{ s}^{-1}$, and the stellar rotation frequency $\Omega = 1.3 \times 10^{-5} \text{ s}^{-1}$ corresponds to a rotation period of 5.6 days.

We normalize radius, time, velocity, density, temperature, pressure, and magnetic field, respectively, as follows:

$$r = \hat{r} r_0, \quad r_0 = R_*, \quad (22)$$

$$t = \hat{t} t_0, \quad t_0 = \sqrt{\frac{r_0^3}{GM_*}}, \quad (23)$$

$$v = \hat{v} v_0, \quad v_0 = \frac{r_0}{t_0}, \quad (24)$$

$$\rho = \hat{\rho}\rho_0, \quad \rho_0 \text{ input parameter}, \quad (25)$$

$$T = \hat{T}T_0, \quad T_0 = \frac{v_0^2}{\mathcal{R}}, \quad (26)$$

$$p = \hat{p}p_0, \quad p_0 = \frac{\mathcal{R}\rho_0}{T_0}, \quad (27)$$

$$B = \hat{B}B_0, \quad B_0 = v_0\sqrt{4\pi\rho_0}. \quad (28)$$

The domain of the integration has four boundaries: the inner and outer radii, the equator, and the axis of rotation. At the inner boundary, the azimuthal velocity component is kept fixed to match the stellar rotation period. For the meridional part of the velocity field, an outflow boundary condition is imposed; i.e., the tangential component of the velocity is assumed continuous, while the vertical component is either continuous (if directed outward) or 0 (otherwise). The azimuthal components of both the magnetic and the electric fields and all scalar quantities are continuous. Imposing the boundary condition on the azimuthal component of the electric field rather than the poloidal magnetic field ensures that the magnetic field remains divergence free. At the outer boundary, the same boundary conditions hold as at the inner boundary, except for the azimuthal velocity component, which is continuous rather than fixed. The boundaries at the axis of rotation and the equator are not real boundaries but an axis and a plane of symmetry, respectively. The boundary conditions therefore all follow from symmetry.

3. RESULTS

We start with a pure MHD model; i.e., equation (10) is used for calculating the start solution only (model A). We have made runs for field strengths B_0 of 100 G, 1 kG, and 10 kG. While our focus is on the 1 kG case, which is closest to observations, the 100 G and 1 kG cases can be regarded as representing the limiting cases of very weak and very strong fields, respectively. Figure 1 shows the evolution of the system in the $B_* = 1$ kG run. Because of the open boundary condition at the inner boundary, the halo is not in hydrostatic equilibrium. A Bondi-type spherically symmetric accretion flow therefore develops immediately after the start of the run, squeezing the stellar dipole by dragging the field inward. Beginning at the inner edge of the disk, the field lines in the halo start to bend outward. Field loops are stretched in the radial direction, and the radial component begins to dominate the poloidal field. Within these elongated loops the gas moves radially outward. The field loops eventually break up when they reach the boundary, leaving parts of the disk disconnected from the star. At $t = 100$ the polar caps of the star as well as most of the disk are threaded by open field lines. Inside the disk the magnetic field is mainly vertical, and its orientation does not vary with the radius. Above the disk there are two areas of strong poloidal field of opposite orientation, with a neutral zone in between, at midlatitudes. As the run proceeds, the neutral zone becomes very narrow, and the distribution of field lines over latitude is roughly flat.

Figure 2 shows the inner region of the system at the beginning and the end of the run. In the vicinity of the inner boundary, the density has increased at all latitudes. The halo is now divided into two regions: a high-density region close to the star and directly above the disk and a low-density area.

At midlatitudes an outflow from the high-density region expands into the low-density region, while at high latitudes the high-density region accretes gas from the low-density region. The gap between the inner edge of the disk and the inner boundary that was present in the initial model has been closed. The density stratification of the innermost part of the disk strongly deviates from the original standard disk and shows a region of high-density inflow on top of a layer with lower density. The poloidal magnetic field structure is still close to the original dipole close to the inner boundary but deviates substantially at midlatitudes and in the upper layers of the disk and the layer immediately above.

The left panel of Figure 3 shows the value of the plasma β ,

$$\beta = \frac{8\pi p_{\text{gas}}}{B^2}, \quad (29)$$

and the toroidal field component. Here $\beta < 1$ in the disk and the high-density part of the halo, and $\beta > 1$ in the low-density region, indicating that the latter is dominated by the magnetic field. In the region shown, which is almost entirely within the corotation radius, the toroidal field is predominantly positive in the northern and negative in the southern hemisphere. Together with a poloidal field that points away from the star in the northern and toward the star in the southern hemisphere, the resulting magnetic torque is negative (transport toward the star).

Figure 4 shows the magnetic field geometries and density distributions for 100 G and 10 kG at $t = 679$ and 173, respectively. The simulation time was limited by technical requirements. Strong fields in areas with low density lead to high Alfvén velocities and thus small time steps because of the Courant criterion. For the weak-field case of 100 G, the magnetic field is compressed in the vertical direction by the infalling gas. A current sheet separates a region of infalling gas around the polar axis from the rest of the halo, where the gas moves outward. The inner regions of the disk remain coupled to the star, but open field lines originate from the outer parts of the disk. The field orientation is essentially vertical inside the disk but almost horizontal above. The disk structure is not changed significantly, but there is a halo around the star with a radius of about 5 stellar radii. In the halo, about 3 stellar radii above the equatorial plane, a current sheet separates the regions of closed and open field lines.

In the 10 kG strong-field case, the inner parts of the disk are disrupted. Beginning at the inner boundary, the gas begins to flow along the magnetic field lines rather than remain in the disk. The inner edge of the disk then moves outward to 10 stellar radii, roughly twice the corotation radius. The accretion flow is vertical at the inner edge of the disk but essentially horizontal closer to the star and reaches the inner boundary of the integration volume at midlatitudes. Between the inner edge of the disk and the inner boundary, a halo forms. Field lines originating from the polar caps of the star open, leaving the outer parts of the disk disconnected from the star, as in the weak-field case. Directly above the disk and at midlatitudes there are two distinct regions of fast outflow with high mass density. The mass loss through the outer boundary amounts to 30% of the accretion rate at the inner boundary. This is, however, still a transient state.

The pure MHD model contains viscous heating terms but no radiative cooling. While this is not an issue for short

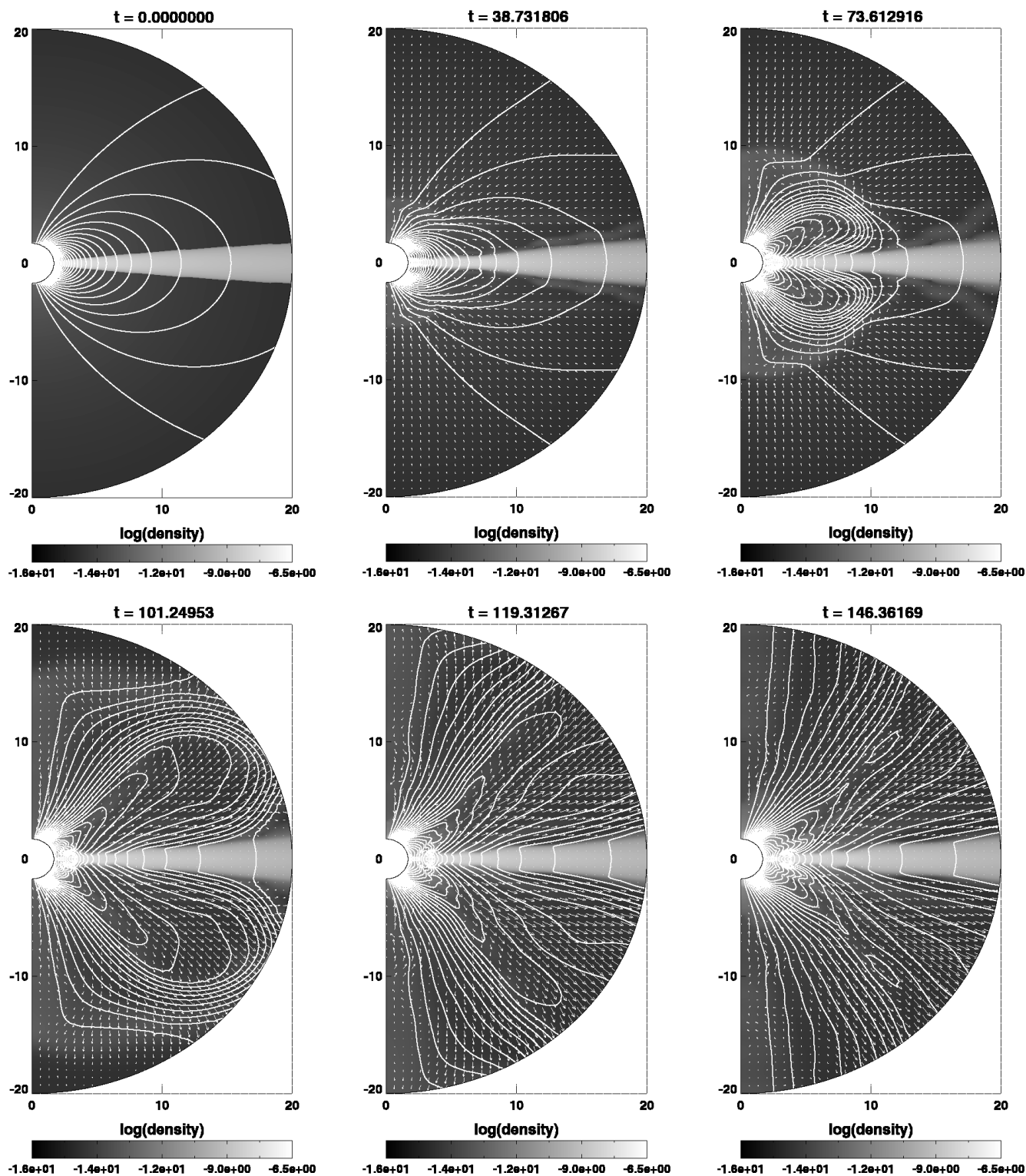


FIG. 1.—Evolution of the magnetic field and the density distribution for model A with a dipole field strength of 1 kG. The diagrams show the system at $t = 0, 39, 75, 101, 119,$ and 146 , respectively, from top left to bottom right. The white solid lines denote field lines, and the arrows the poloidal component of the gas velocity. [See the electronic edition of the *Journal* for a color version of this figure.]

simulation times, it might prevent the system from reaching an equilibrium. We therefore study a second model (model B) using the same start solution but keeping the radiation transport switched on, i.e., solving equation (10) together with equations (2)–(5). We again make runs with 100 G, 1

kG, and 10 kG. Figure 5 shows the density, poloidal field, and (meridional) gas flow for the extreme cases of 100 G and 10 kG.

As in the pure MHD case, the weak field (100 G) is squeezed by the gas infalling from the halo. A sheet of open

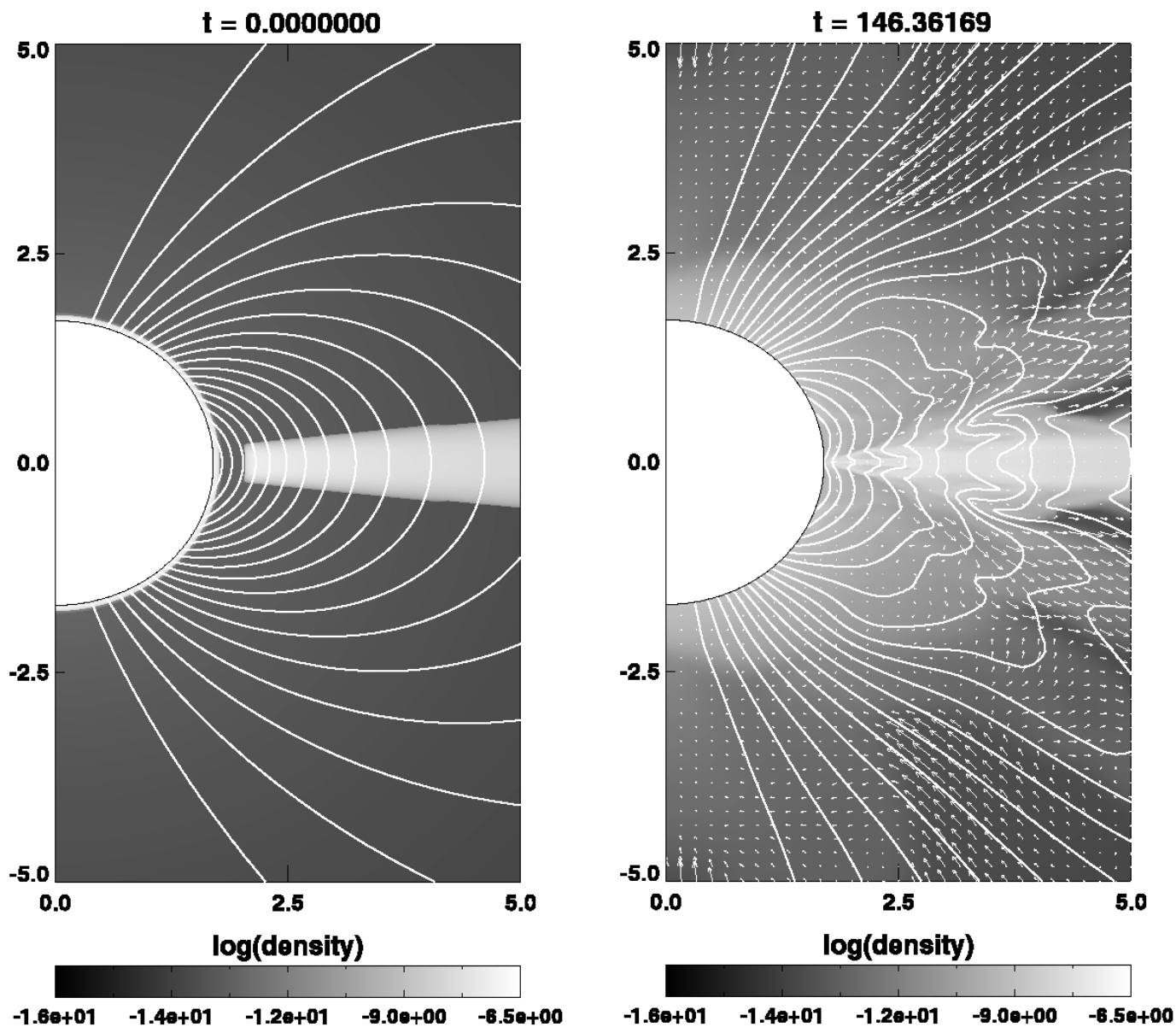


FIG. 2.—Innermost region of the disk for $B_* = 1$ kG, model A. *Left*: Initial density distribution and poloidal magnetic field. *Right*: Density distribution, poloidal magnetic field, and meridional gas flow at $t = 146$. [See the electronic edition of the *Journal* for a color version of this figure.]

field lines develops that separates the area close to the rotation axis from the rest of the halo. The inner parts of the disk are coupled to the star, while the outer parts are threaded by open field lines. The transition between both regions occurs at 8 stellar radii. Above the outer parts of the disk, field lines are bent outward and their orientation is roughly parallel to the disk surface. The halo is almost neutral at midlatitudes, where a slow outflow occurs.

A very strong field of 10 kG disrupts the disk within 8 stellar radii. Field lines originating from the polar caps of the star are open, while those with footpoints closer to the equator are closed. A high-density outflow emerges at midlatitudes. Between the inner boundary and the inner edge of the disk, the region of maximum density lies at about 1.5 stellar radii above the equatorial plane. The magnetic field is bent inward below and outward above the region of maximal density.

The 1 kG case is shown in Figure 6. The density distribution differs considerably from the pure MHD case. The innermost part of the disk has become very thin, and a small gap is present between the inner edge of the disk and the inner boundary. The almost spherical halo around the inner boundary found in the pure MHD model is missing. Instead, a high-density region has formed above the disk, extending about 15° in latitude, with densities between 1 and 2 orders of magnitude lower than inside the disk. Gas accretion through the inner boundary takes place through this halo rather than the disk. The poloidal field structure is similar to that found with model A, but the closed field line region extends about twice as far in the disk plane, to about 8 stellar radii. The field lines threading the outer disk are still bent outward, but not as strongly as in the weak-field case.

The toroidal field and plasma β for this case are shown in the right panel of Figure 3. As in model A, $\beta > 1$ in the disk

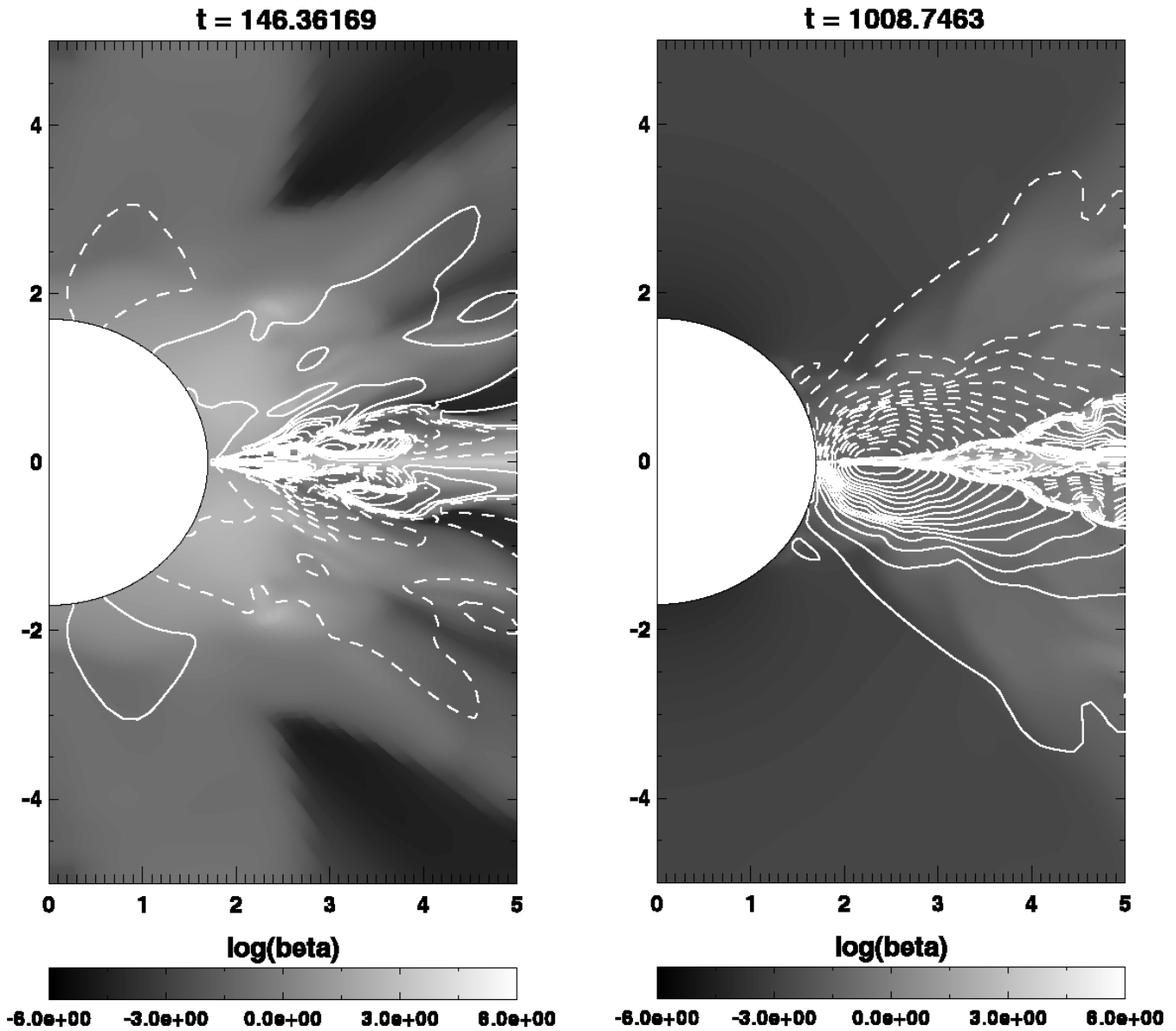


FIG. 3.—Plasma β and toroidal magnetic field for the $B_* = 1$ kG runs of models A (left) and B (right). Solid lines denote positive values of B_ϕ , and broken lines negative values. [See the electronic edition of the *Journal* for a color version of this figure.]

and high-density region of the halo, and $\beta < 1$ elsewhere. The toroidal field distribution, however, is completely different. Inside the disk, B_ϕ is positive in the upper and negative in the lower part of the disk but has reversed signs in the halo above. This leads to opposite toroidal field polarities on the inner boundary for the two models.

4. DISCUSSION

Our computations show that the initial configuration with a dipolar magnetic field rooted in a star surrounded by a Keplerian disk is unstable. Unless the field strength on the stellar surface exceeds a certain threshold of several kilogauss, the field in the halo above the disk is wound up because of the different rotation rates of the footpoints of each field line. A toroidal field is generated, and the poloidal field lines are stretched in the radial direction at midlatitudes. Field lines originating from the equatorial regions of the stellar surface remain closed, while those originally con-

necting the polar caps of the star with the outer parts of the disk break up, leaving star and disk threaded by open field lines. For field strengths above the threshold value, the inner parts of the disk are disrupted, and the accretion flow changes from disk to magnetospheric accretion. For the disk studied here with an accretion rate of $10^{-7} M_\odot \text{ yr}^{-1}$ and a viscosity parameter $\alpha_{\text{SS}} = 0.01$, surrounding a solar-mass star with a radius of $3 R_\odot$, the critical field strength lies between 1 and 10 kG, measured on the stellar surface. For field strengths below the threshold value, the disk height decreases inside the corotation radius. The magnetocentrifugal force exerted by the wound-up field drives an outflow at midlatitudes. The mass-loss rate varies strongly with time. It can reach a significant fraction of the mass accretion rate and temporarily even exceed it. Outflow velocities reach up to 200 km s^{-1} at a 20 stellar radii distance from the star, which exceeds the escape velocity of 60 km s^{-1} . Because of the open boundaries, our setup does not guarantee the existence of a stationary solution. As a consequence, none of

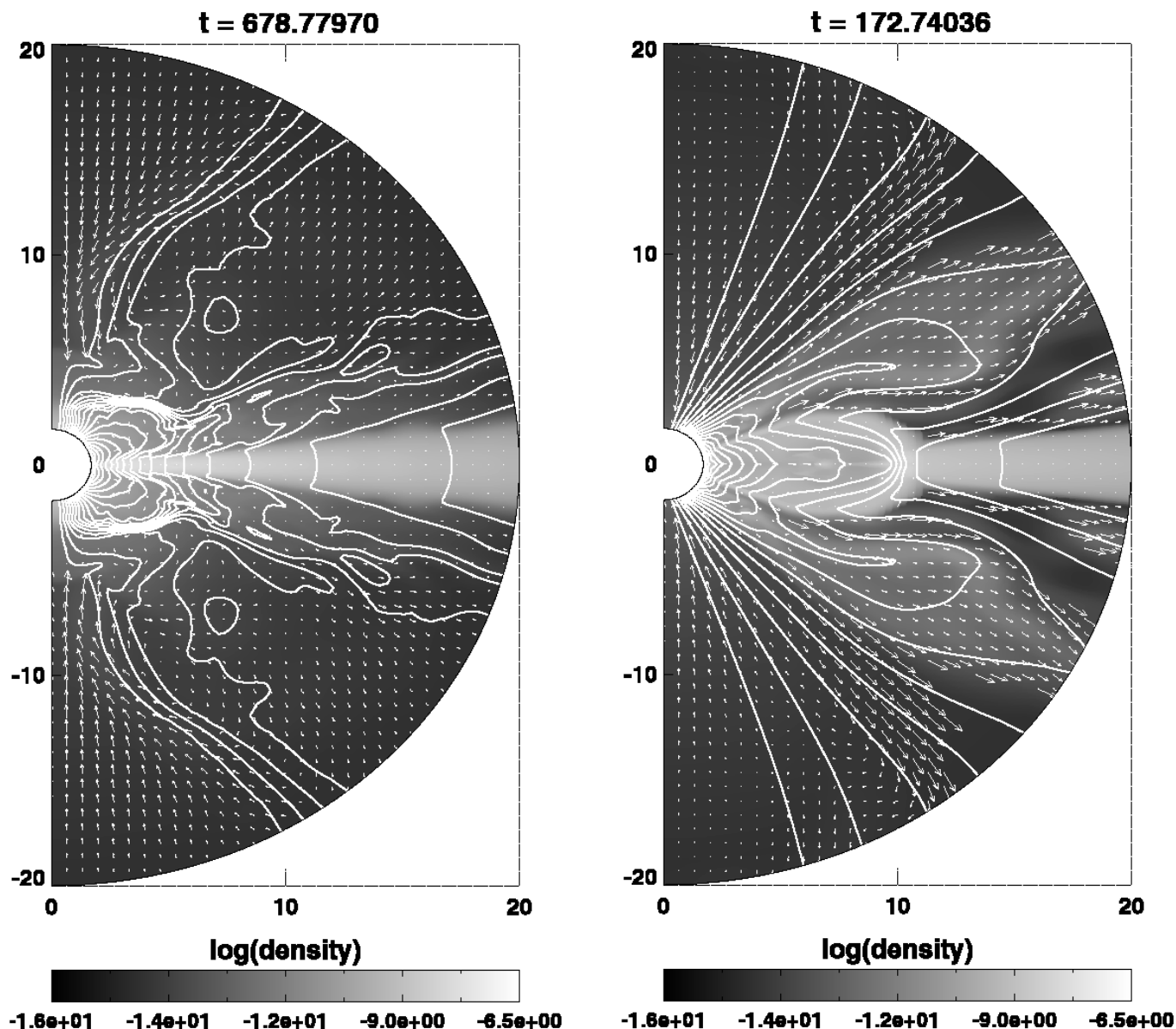


FIG. 4.—Weak- and strong-field cases for model A. *Left:* For $B_* = 100$ G. *Right:* For $B_* = 10$ kG. [See the electronic edition of the *Journal* for a color version of this figure.]

our runs reached a stationary state. In the $B_* = 100$ G model B case, which was run longest, the solution became stationary in a statistical sense in the inner parts of the simulation volume.

In contrast to pure MHD models usually focused on jet collimation, both the disk and the halo are relatively cool in our model (except in the vicinity of the inner boundary in model A), with initial temperatures of a few thousand kelvins only. We have taken into account the low degree of ionization at these temperatures in the equation of state only and have assumed that the equations of MHD still hold. At the limited resolution of our computations, eddy viscosity and magnetic diffusivity coefficients have to be used rather than their molecular counterparts anyway, and one can hope that the turbulent diffusion processes do not strongly depend on the molecular viscosity and ohmic resistivity, if the latter exist at all.

The most striking difference between the models with and without radiation is the structure of the halo. Model A

shows a high-density region around the central star with temperatures up to 10^6 K. Model B lacks this halo around the star and has a region of increased density above the disk instead, and lower temperatures in the halo compared to model B. In the runs with radiation transport switched on, the disk showed a tendency to thicken, especially in the outer parts, temporarily reaching an H/R aspect ratio of about 1 in some cases. A run with zero field strength showed that this behavior is not caused by the magnetic field but appears to be a consequence of the rather moderate density contrast between disk and halo chosen to limit the Alfvén speed. An inspection of the halo's thermal properties revealed that the disk became unstable whenever the gas temperature in the halo was between 5000 and 10,000 K, at which the opacity is a rapidly increasing function of the temperature, a condition known to cause disk instability.

The ratio of poloidal to toroidal field energies is less than 1 in all runs, increasing from 0.01 for a polar field strength of 100 G to 1 in the 10 kG case. This is probably due to the

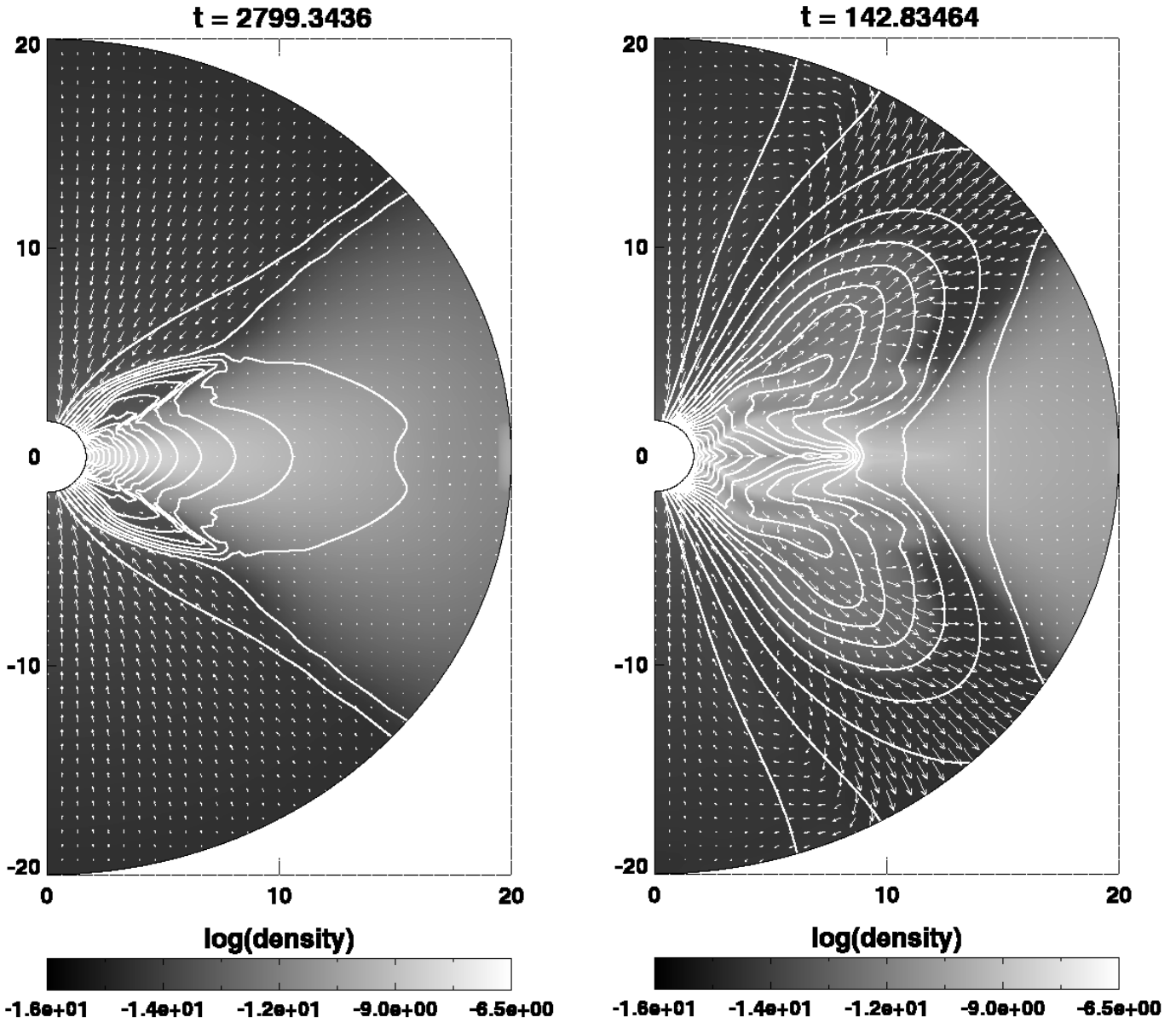


FIG. 5.—Density, poloidal field lines, and meridional gas motion for the weak- and strong-field cases of model B. *Left:* For $B_* = 100$ G. *Right:* For $B_* = 10$ kG. [See the electronic edition of the Journal for a color version of this figure.]

fact that the force necessary to adjust the accretion flow to the magnetic field depends on the densities of mass and kinetic energy in the disk, which are always roughly the same.

We now address the problem of angular momentum transport. The azimuthal component of the equation of motion expresses the conservation of angular momentum:

$$r^2 \sin^2 \theta \rho \frac{\partial \Omega}{\partial t} = \nabla \cdot \mathbf{t} . \quad (30)$$

The magnetic contribution to the transport vector is

$$\mathbf{t}_{\text{mag}} = \frac{r \sin \theta B_\phi}{4\pi} \mathbf{B} , \quad (31)$$

and the total torque is given by the surface integral

$$T_{\text{mag}} = 2\pi r^2 \int_0^\pi (\mathbf{t}_{\text{mag}} \cdot \mathbf{r}) \sin \theta d\theta . \quad (32)$$

Defined as in equation (32), the torque is positive when angular momentum is extracted from the star and negative when the stellar rotation is accelerated. The initial configuration always produces a negative torque.

With model A, the torque was found to be negative in the 100 G and 1 kG runs and positive in the 10 kG run. Figures 7 and 8 show the poloidal and toroidal field energies as well as the magnetic torque as functions of time for model B and values of 100 G and 1 kG, respectively. In both cases, the total torque is negative at the beginning⁴ and strongly varies with time, even changing its sign, but becomes more steady after $t = 1000$ and 500 , respectively, and the sign is positive most of the time. In the $B_* = 100$ G case, the poloidal field energy, magnetic torque, and kinetic energy become

⁴ The initial phase is not shown in the $B_* = 1$ kG case because of some high (negative) peaks in the magnetic torque curve.

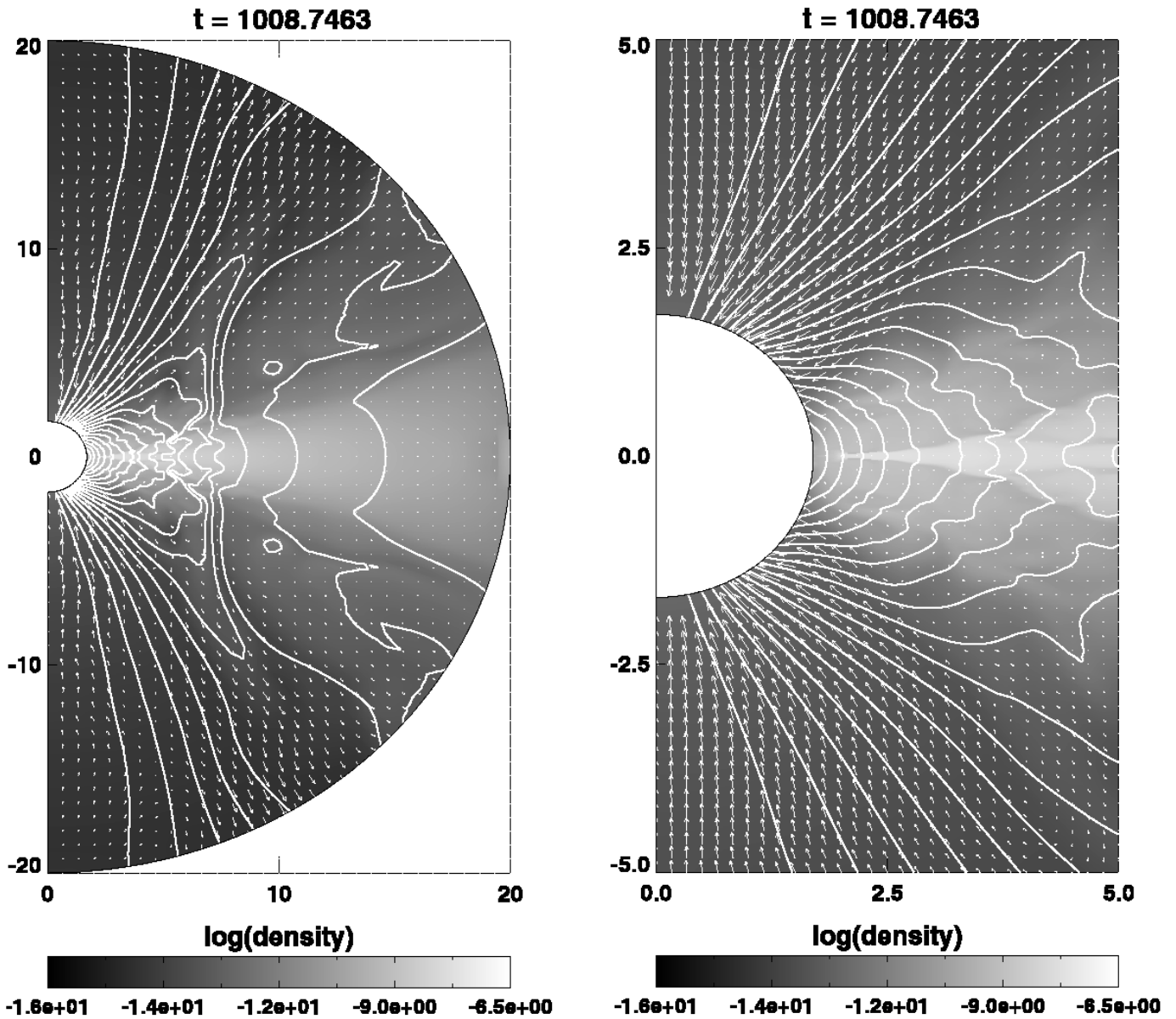


FIG. 6.—Density, poloidal magnetic field, and velocity for $B_* = 1$ kG, model B. The right panel is an enlarged view of the inner part of the left. [See the electronic edition of the *Journal* for a color version of this figure.]

essentially constant after $t = 1000$, but the toroidal field energy continues to grow. This is due to the longer timescale for the toroidal field evolution in the outer parts of the disk, which do not contribute significantly to the magnetic torque.

The surprising positive sign of the torque is a consequence of the negative sign of the toroidal field component in the upper hemisphere and the positive sign in the lower hemisphere, at the inner boundary. The high-density region of the halo corotates with the disk. In this region, the dominating generator of the toroidal field is the radial shear term in the induction equation,

$$\sin \theta B_r \frac{\partial \Omega}{\partial r},$$

which is negative for positive B_r and Keplerian rotation. At the boundary, there is a sharp increase of the rotation rate,

generating a toroidal field of the opposite sign. For the flux generated in this boundary layer to penetrate the disk, the timescale of radial field diffusion,

$$\tau_{\text{diff}} = \frac{l^2}{\eta}, \quad (33)$$

must be shorter than the timescale of field advection,

$$\tau_{\text{adv}} = \frac{l}{u_r}. \quad (34)$$

With values of 10^{11} cm for the length scale l , 10^{14} cm² s⁻¹ for the magnetic diffusivity η , and 10^7 cm s⁻¹ for the radial velocity component, $\tau_{\text{diff}} = 10^8$ s, while $\tau_{\text{adv}} = 10^6$ s. The positive radial shear at the inner boundary, although very strong, is therefore without effect, because the flux it generates is immediately removed from the integration volume.

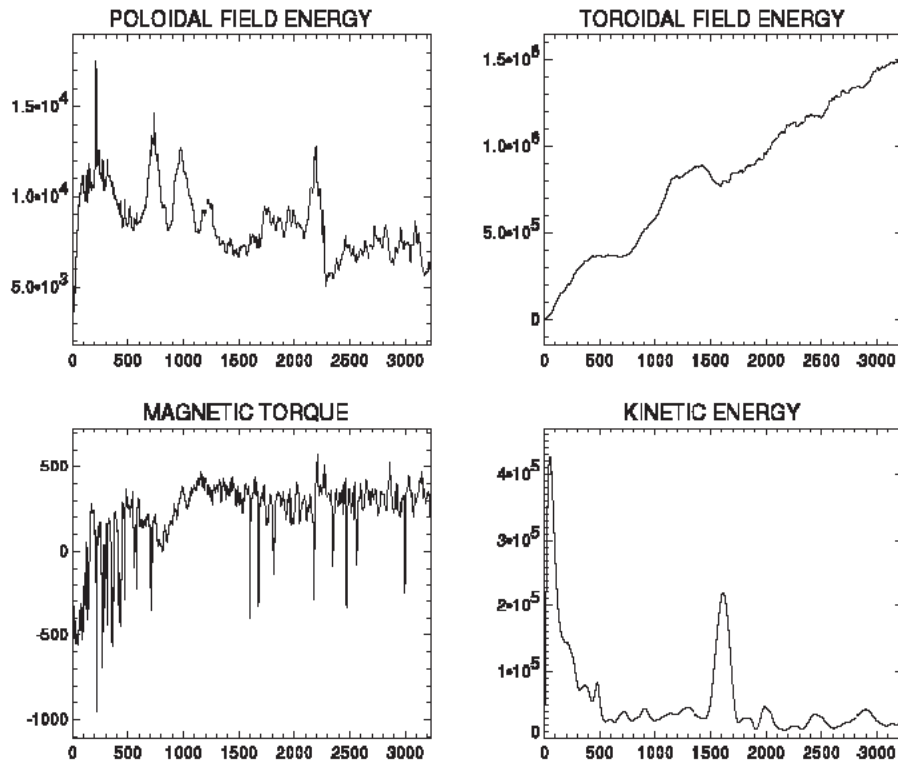


FIG. 7.—Poloidal and toroidal field energies and magnetic torque as functions of time for the model B, $B_* = 100$ G case. The units of the energies are arbitrary, and the torque is in cgs units, divided by R_*^3 . Positive torque means angular momentum transport in the *positive* r -direction, *away from the star*.

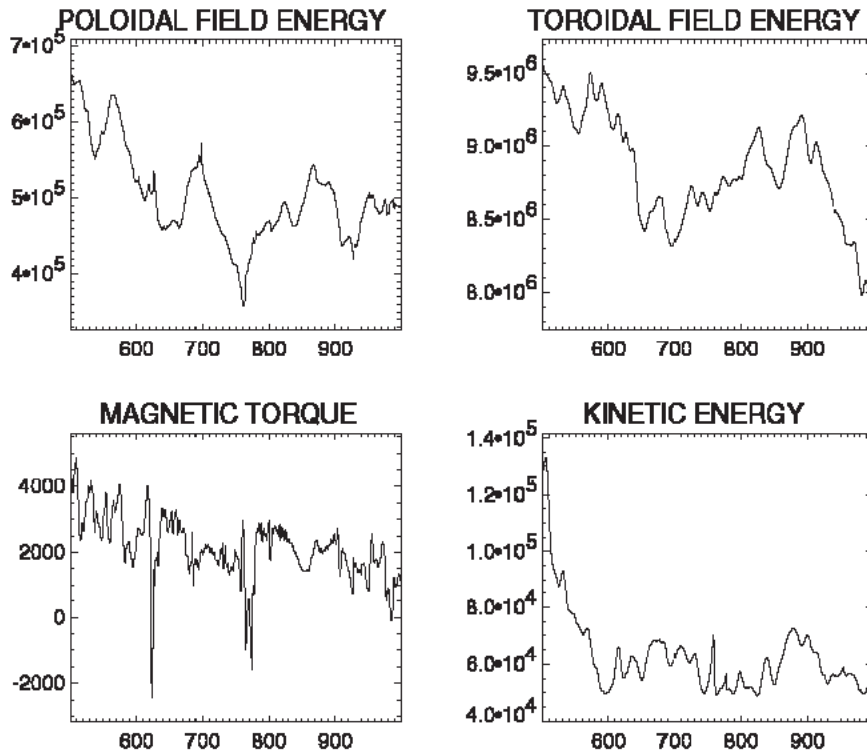


FIG. 8.—Same as Fig. 7, but for $B_* = 1$ kG

The timescale for the spin-down of a star rotating with angular frequency Ω is given by the relation

$$I\dot{\Omega} = T, \quad (35)$$

where

$$I = \frac{8\pi}{3} \int_0^R \rho r^4 dr = Mk^2 R^2 \quad (36)$$

is the star's moment of inertia and k the fractional radius of gyration. The value of k depends on the density stratification. We use $k^2 = 0.2$, as derived from polytrophic models for fully convective stars (Rucinski 1988). For a solar-mass T Tauri star, $M = 2 \times 10^{33}$ g and $R = 2 \times 10^{11}$ cm, equation (36) yields a value of 1.6×10^{55} g cm². The spin-down timescale is given by

$$\tau = \frac{\Omega}{\dot{\Omega}}. \quad (37)$$

In the 1 kG run, the value of the magnetic torque is of the order of 2×10^{37} g cm² s⁻², which would give a spin-down time of about 3 Myr. However, by comparison of the magnetic torque with the accretion torque,

$$T_{\text{acc}} = 2\pi r^2 \int_0^\pi (u_r \Omega \rho r^2 \sin^2 \theta) r \sin \theta d\theta, \quad (38)$$

we find a value of 2.7×10^{39} g cm² s⁻² for the latter, exceeding the magnetic torque by 2 orders of magnitude. The total torque at the inner boundary is thus always negative, spinning up the star.

For magnetic field strengths of the order of 1 kG, our model produces outflows at midlatitudes, but no collimation occurs. Although both the mass accretion rate and the total magnetic torque vary strongly with time, we did not encounter periodic or quasi-periodic behavior, as reported by Goodson & Winglee (1999, hereafter GW99) and Matt et al. (2002). This discrepancy is most likely due to different choices of the viscosity parameter. While GW99 use a constant value of 5×10^{16} cm² s⁻¹ in their innermost box, ours is smaller by 2 orders of magnitude in the disk, and 0 in the halo. With the magnetic diffusivity parameter set to 0, reconnection can take place because of the numerical diffusion only, which is small compared to the eddy magnetic diffusivity in the disk or the constant value used by GW99.

Shu et al. (1994) find that a stellar magnetic field strong enough to truncate the circumstellar accretion disk is always strong enough to drive a magnetocentrifugal wind with mass-loss rates of the same order as the mass accretion rate of the disk. In their model the truncation radius of the disk, R_t , is somewhat closer to the star than the X-point, R_X , which marks the outer boundary of the zone from which mass can flow onto the star through the funnel flow. Just outside the X-point lies the region where the wind originates. Angular momentum transport from the star to the disk is possible if the magnetic field is strong enough to keep the magnetosphere in corotation with the star. The angular momentum transferred to the disk is then mostly carried away by the wind. For the location of the X-point, they derive the estimate

$$R_X = \Gamma_X R_*, \quad \Gamma_X = \alpha_X \left(\frac{B_*^4 R_*^5}{GM_* \dot{M}^2} \right)^{1/7}, \quad (39)$$

with $\alpha_X < 1$ a dimensionless parameter, which differs from equation (1) only in the value of the dimensionless parameter, which is slightly greater for the X-point than for the truncation radius. With $B_* = 1$ kG, equation (39) yields $\Gamma_X = 4.8\alpha_X$ for our model. That the disk is not truncated at this field strength in our model can thus be easily explained if $\alpha_X < 0.4$, in which case the truncation radius just lies too close to the star. For a field strength of 10 kG, a radius of 7.2 stellar radii would then follow for the X-point. In Figures 4 and 5 the truncation radius is about 10 stellar radii, somewhat larger than predicted by the Shu et al. (1994) model. Since the system is far from stationary, and the elapsed time was not long enough for the field lines to open, we cannot decide how significant this discrepancy is.

5. CONCLUSIONS

We have carried out MHD simulations of an accretion disk around a T Tauri star with an initially dipolar magnetic field to study the field structure in the magnetosphere, the truncation of the disk, and the torque on the star. We have carried out runs with and without radiative energy transport. While in the pure MHD models a hot halo with temperatures up to 10^6 K forms around the star, models including radiation tend to produce cooler magnetospheres with temperatures of a few thousand kelvins and a layer of higher density above the disk, which dominates the accretion flow close to the inner boundary.

For an accretion rate of $10^{-7} M_\odot \text{ yr}^{-1}$ and an inner radius of 1.7 stellar radii, the field strength B_* necessary for disk truncation lies between 1 and 10 kG, in agreement with the purely analytical models by Ghosh & Lamb (1979a) and Shu et al. (1994).

Magnetic fields of the order of 1 kG can drive outflows with mass-loss rates of 1/10 of the disk accretion rate or above. Our results confirm the finding of Shu et al. (1994) that a field strong enough to disrupt the disk is also strong enough to drive an outflow. We have, however, found cases in which the wind exists without disk disruption.

The inner boundary in our simulations is located between the corotation radius and the stellar surface, not *on* the stellar surface. Although the poloidal magnetic flux and the rotation rate are fixed, mass, angular momentum, and toroidal magnetic flux can leave the system through this boundary. For a complete treatment of the angular momentum problem, it is necessary to extend the integration volume down to the stellar surface and find a more realistic boundary condition.

In this study we have explored the types of solution for field strengths covering 2 orders of magnitude for a fixed rotation rate rather than trying to find an equilibrium solution with disk truncation up to the corotation radius. From these results as well as from the analytical models, it is clear that for prescribed mass accretion and stellar rotation rates, such an equilibrium state can only be reached for a unique field strength, which can only be found by either tuning the magnetic field strength for fixed rotation rate or vice versa.

We have found three types of solutions: (1) A weak field is compressed by the infalling gas, and the disk is only weakly

affected. (2) A field of an intermediate strength of 1 kG drives an outflow but is not strong enough to directly disrupt the disk. We cannot exclude the possibility, however, that (3) the inner parts of the disk are slowly drained through magnetically enhanced accretion. A magnetic field

as strong as 10 kG disrupts the disk to radii beyond the corotation radius by pushing the gas outward.

This work was supported by the Deutsche Forschungsgemeinschaft.

REFERENCES

- Agapitou, V., & Papaloizou, C. B. 2000, *MNRAS*, 317, 273
 Alexander, D. R., Augason, G. C., & Johnson, H. R. 1989, *ApJ*, 345, 1014
 Aly, J. J. 1984, *ApJ*, 283, 349
 Armitage, P. J., & Clarke, C. J. 1996, *MNRAS*, 280, 458
 Bardou, A., & Heyvaerts, J. 1996, *A&A*, 307, 1009
 Bell, K. R., & Lin, D. N. C. 1994, *ApJ*, 427, 987
 Bouvier, J., Forestini, M., & Allain, S. 1997, *A&A*, 326, 1023
 Bouvier, J., et al. 1993, *A&A*, 272, 176
 Camenzind, M. 1990, *Rev. Mod. Astron.*, 3, 234
 Cameron, A. C., & Campbell, C. G. 1993, *A&A*, 274, 309
 Edwards, S., et al. 1993, *AJ*, 106, 372
 Elstner, D., & Rüdiger, G. 2000, *A&A*, 358, 612
 Evans, C. R., & Hawley, J. F. 1988, *ApJ*, 332, 659
 Ghosh, P. 1995, *MNRAS*, 272, 763
 Ghosh, P., & Lamb, F. K. 1978, *ApJ*, 223, L83
 ———. 1979a, *ApJ*, 232, 259
 ———. 1979b, *ApJ*, 234, 296
 Goodson, A. P., & Winglee, R. M. 1999, *ApJ*, 524, 159 (GW99)
 Goodson, A. P., Winglee, R. M., & Böhm, K.-H. 1997, *ApJ*, 489, 199
 Guenther, E. W., & Emerson, J. P. 1996, *A&A*, 309, 777
 Guenther, E. W., Lehmann, H., Emerson, J. P., & Staude, J. 1999, *A&A*, 341, 768
 Hawley, J. F., & Stone, J. M. 1995, *Comput. Phys. Commun.*, 89, 127
 Johns-Krull, C. M., Valenti, J. A., & Koresko, C. 1999, *ApJ*, 516, 900
 Kitchatinov, L. L., Pipin, V. V., & Rüdiger, G. 1994, *Astron. Nachr.*, 315, 157
 Klahr, H. H., Henning, Th., & Kley, W. 1999, *ApJ*, 514, 325
 Kley, W. 1989, *A&A*, 222, 141
 Königl, A. 1991, *ApJ*, 370, L39
 Levermore, C. D., & Pomraning, G. C. 1981, *ApJ*, 248, 321
 Li, J., Wickramasinghe, D. T., & Rüdiger, G. 1996, *ApJ*, 469, 765
 Lovelace, R. V. E., Romanova, M. M., & Bisnovatyi-Kogan, G. S. 1995, *MNRAS*, 275, 244
 Matt, S., Goodson, A. P., Winglee, R. M., & Böhm, K.-H. 2002, *ApJ*, 574, 232
 Miller, K., & Stone, J. M. 1997, *ApJ*, 489, 890
 Rucinski, S. M. 1988, *AJ*, 95, 1895
 Shakura, N. I., & Sunyaev, R. A. 1973, *A&A*, 24, 337
 Shu, F., et al. 1994, *ApJ*, 429, 781
 Stassun, K. G., et al. 1999, *AJ*, 117, 2941
 ———. 2001, *AJ*, 121, 1003
 Stone, J. M., & Norman, M. L. 1992a, *ApJS*, 80, 753
 ———. 1992b, *ApJS*, 80, 791
 ———. 1994, *ApJ*, 433, 746
 Uchida, Y., & Shibata, K. 1985, *PASJ*, 37, 515
 Weber, E. J., & Davis, L. 1967, *ApJ*, 148, 217
 Yi, I. 1994, *ApJ*, 428, 760